Applied Surface Science 620 (2023) 156779

Contents lists available at ScienceDirect

Applied Surface Science

journal homepage: www.elsevier.com/locate/apsusc

Full Length Article

Optical sensing and switching in the visible light spectrum based on the bound states in the continuum formed in GaP metasurfaces

Zhaotang Li [a], Mingcheng Panmai [a], Lidan Zhou [a,b], Shulei Li [a,c], Shimei Liu [a], Jianhua Zeng [d], Sheng Lan [a,*]

[a] Guangdong Provincial Key Laboratory of Nanophotonic Functional Materials and Devices, School of Information and Optoelectronic Science and Engineering, South China Normal University, Guangzhou 510006, China
[b] State Key Laboratory of Optoelectronic Materials and Technologies, School of Electronics and Information Technology, Sun Yat-sen University, Guangzhou 51006, China
[c] School of Optoelectronic Engineering, Guangdong Polytechnic Normal University, Guangzhou 510665, China
[d] School of Physics and Electronic Information, Shangrao Normal University, Shangrao 334001, China

ARTICLE INFO

Keywords:
Dielectric metasurface
Bound state in the continuum
Gallium phosphide nanoparticle
Mie resonance

ABSTRACT

We propose dielectric metasurfaces supporting BICs in the visible light spectrum based on GaP cuboids. An artificial "molecule" composed of two identical GaP cuboids, which exhibits highly directional scattering, is used as the unit cell to construct the metasurfaces. It is found that the Q factor of the BIC is extremely sensitive to the gap width between the two GaP cuboids. A Q factor as high as 2×10^7 can be achieved when the gap width of all GaP cuboids in the metasurface becomes equal. An exponential decrease in the Q factor is observed when the gap width deviates from the optimum value. We show that optical sensing with sensitivities of 135 nm/RIU and 45 nm/RIU can be realized by using *x*-and *y*-polarized white light. By integrating a tungsten disulfide (WS_2) monolayer on such a metasurface, we demonstrate that the BIC in the hybrid metasurface can be optically manipulated by injecting excitons and trions in the WS_2 monolayer. Our findings are helpful for understanding the physical origin for the BIC formed in a metasurface and useful for constructing novel photonic functional devices by combining such metasurfaces with two-dimensional materials.

1. Introduction

Metasurfaces composed of periodically arranged elements have attracted great interest in recent years because of their abilities in controlling the optical properties of electromagnetic wave, such as amplitude, phase, wavefront, and polarization [1–5]. Although all-metallic metasurfaces have been successfully employed to manipulate the optical properties of light, it is difficult to obtain optical resonances with high quality (Q) factors in the visible light spectrum because of the large Ohmic loss of metals [6–8]. For this reason, all-dielectric metasurfaces composed of dielectric nanoparticles with high refractive indices have become the focus of many studies because they support bound states in the continuum (BICs) with high Q factors, which imply potential applications in various fields [9–16]. Physically, BICs with infinitely large Q factors exist only in metamaterials with infinite size at least in one dimension, such as a two-dimensional metamaterial or a metasurface with infinite size [17–20]. They are generally clarified into two types which are referred to as symmetry-protected BICs [11,12,14] and accidental (or F-W) BICs [21–24]. The former BICs are decoupled with the radiation continuum by the symmetry of the constituent elements (or dielectric nanoparticles) with respect to the incident light by exploiting mainly the dark axis of electric or magnetic dipoles [14,16,25]. Breaking of symmetry can be realized by using oblique incidence or by introducing defects in dielectric nanoparticles [25–27]. As a result, quasi-BICs with reduced Q factors can be readily excited in the metasurface. It is generally accepted that symmetry-protected BICs cannot be excited unless the symmetry is broken [25,28]. For the symmetry-protected BIC generated by a dielectric cylinder or block, it is revealed that its radiation is governed by a magnetic dipole (MD) parallel to the direction of the light incidence, which appears as a doughnut perpendicular to the incident light.

Physically, the transmission or reflection of a metasurface is determined by the scattering of the constituent elements and the coherent interaction between them. Therefore, it becomes important to study the

* Corresponding author.
E-mail address: slan@scnu.edu.cn (S. Lan).

https://doi.org/10.1016/j.apsusc.2023.156779
Received 19 December 2022; Accepted 14 February 2023
Available online 17 February 2023

scattering of the unit cell used to construct the metasurface. As mentioned above, the symmetry-protected BICs reported in previous studies are usually dominated by MDs oriented in the direction of light incidence. Such a MD is supported by a single dielectric element, such as a cylinder or a cuboid. Based on previous studies, normally incident light can be deflected by using an artificial "molecule" consisting of two Si nanoparticles [29,30]. It is realized by exploiting the constructive and destructive interference between the Mie resonances supported by such an artificial "molecule" [29]. If a large deflection angle of 90° can be achieved, it implies the disappearance of the transmitted light or the existence of an optical resonance with an infinitely large Q factor in the transmission spectrum. In this case, the Si dimer is decoupled with the radiation continuum, generating a BIC without breaking the geometrical symmetry. Actually, it was demonstrated that such a situation can be realized in an artificial "molecule" consisting of two Si nanospheres. When such a Si "molecule" is irradiated by using a radially-polarized light beam, a sharp bending of the light beam with an angle of 90° can be observed [30]. The underlying physical mechanism is the destructive interference between the toroidal electric dipole (TD) and the magnetic quadrupole (MQ) excited in the Si "molecule" in the direction of light incidence. In this case, a sharp bending of the incident light is realized, leading to a bidirectional scattering perpendicular to the incident light. Enlightened by this phenomenon, it is expected that a dielectric metasurface composed of periodically arranged dielectric "molecule" may support a symmetry-protected BIC of a different nature.

From the viewpoint of practical application, the high-Q optical resonances formed in a metasurfaces, such as the BICs, can be employed to realize optical sensing with high sensitivities. In practice, optical sensing based on the modifications in the spectral shape, resonant wavelength and intensity of an optical resonance induced by the variation in the dielectric environment has been successfully demonstrated [31–36]. For the BIC formed in a metasurface, its resonant wavelength usually exhibits a strong dependence on the refractive index of the surrounding environment because of the strong localization of the electric field in the unit cell. This feature is commonly exploited to realize optical sensing. On the other hand, the high Q factor of the BIC implies a high sensitivity or a large figure of merit (FOM) for the optical sensor.

Physically, an optical resonance with a high Q factor implies significantly enhanced interaction with light. Therefore, a dielectric metasurface is usually employed to enhance the linear and nonlinear optical responses of a two-dimensional material or a perovskite thin film, which can be readily integrated on the dielectric metasurface [37–39]. For example, it was found that the second harmonic generation is greatly enhanced by placing a WS_2 monolayer on a Si-based metasurface and exciting the WS_2 monolayer at the BIC of the metasurface [37]. On the other hand, the BIC should be quite sensitive to the small variation of the dielectric constant of the surrounding environment. For example, a small increase in the imaginary part of the dielectric constant of the dielectric nanoparticle by optically induced free carriers [40,41] or the surrounding environment by adding a graphene on top of the metasurface will lead to a dramatic reduction or even the disappearance of the BIC [13]. This unique feature offers us the opportunity for manipulating the BIC of a dielectric metasurface with an attached two-dimensional material through injecting excitons and trions with laser light. Since the exciton resonances for many commonly used two-dimensional materials (e.g., WS_2 and MoS_2) or perovskites (e.g., $CsPbBr_3$) are located in the visible light spectrum, it is highly desirable to seek a semiconductor with a negligible loss in this regime. Unfortunately, Si-based metasurfaces cannot support BICs with high Q factors in the visible light spectrum because its imaginary part is not sufficiently small [42].

In this article, we propose a GaP-based metasurface that supports a BIC in the visible light spectrum. We reveal that the BIC originates from the interference of the Mie resonances supported by a GaP "molecule" composed of two identical GaP cuboids. We find that the Q factor of the BIC depends exponentially on the gap width between the GaP cuboids and the maximum value is achieved when the gap width of neighboring GaP cuboids becomes equal. We show that optical sensing with FOM larger than 10^6 can be realized by using such GaP-based metasurfaces. We demonstrate numerically that the BIC in a WS_2/GaP hybrid metasurface can be optically manipulated by injecting excitons and trions in the attached WS_2 monolayer.

2. Materials and methods

Numerical Simulation: In this work, we used a multi-physics software (COMSOL) to study metasurfaces with infinite sizes. In the numerical simulation, a periodical boundary condition was employed in the x and y directions and perfectly matched layers in the z direction to absorb the outgoing waves. In all cases, we used a plane wave propagating in the z direction to excite the metasurface. The complex refractive index of GaP was taken from literature [43] while that of SiO_2 was set to be 1.45. We calculated the transmission spectra of the metasurfaces and simulated the electric field distribution and radiation pattern of the GaP "molecule" used to construct the metasurfaces in the wavelength domain. The Q factor of the quasi-BIC supported by a metasurface was derived from the complex eigen-frequency, which can be expressed as $\omega_0 + i\gamma$. Here, ω_0 and γ denote the real and imaginary parts of the complex eigen-frequency. The Q factor was derived by

$$Q = \omega_0/2\gamma \quad (1)$$

3. Results and discussion

3.1. BICs formed in GaP-based metasurfaces

We started from a detailed comparison of the complex refractive indices of Si and GaP in the wavelength range of 500–800 nm, as shown in Fig. 1a and 1b. It is noticed that the real part of the refractive index of Si is reduced from 4.3 to 3.7 while that of GaP is reduced from 3.6 to 3.2 in this wavelength range. Although the refractive index of GaP is smaller than that of Si, its value is large enough to support distinct Mie resonances in the visible to near infrared spectral range. In Fig. 1b, it is observed that the extinction coefficient of Si is reduced from 0.07 to 0.006. This value originates from the indirect bandgap absorption of Si and it is small enough to support Mie resonances with finite Q factors. However, this value is not sufficiently small to sustain BICs with high Q factors because a small increase in the extinction coefficient will lead to a dramatic reduction in the Q factors of the BICs. In sharp contrast, it is remarkable that the extinction coefficient of GaP becomes zero for wavelengths longer than ~ 560 nm. It implies that a metasurface built with GaP nanoparticles may support optical resonances with extremely large Q factors, such as BICs.

In Fig. 1c, we show schematically the configuration of a GaP-based metasurface proposed and studied in this work. It is excited by using a plane wave propagating along the $-z$ direction and polarized along the y direction. The GaP metasurface is constructed by a square lattice of GaP "molecules", each of which is formed by two identical GaP cuboids, as shown in Fig. 1d. From the viewpoint of practical application, the GaP metasurface can be fabricated on a SiO_2 substrate by using wafer bonding, electron lithography and reactive ion etching [44]. In Fig. 1d, we depict the geometrical parameters characterizing the GaP "molecule", including the length (l), width (w), and height (h) of the GaP cuboid, the gap width (g) between the two GaP cuboids, and the period (p) of the square lattice.

We first examine the high-Q optical resonance appearing in the transmission spectrum of a GaP metasurface with $p = 310$ nm, $l = 240$ nm, $w = 110$ nm, $h = 150$ nm, and $g = 40$ nm, as shown in Fig. 1e. It is noticed that the optical resonance exhibits a typical Fano lineshape, which is generally formed by the interference of two optical modes. This optical resonance is intentionally designed at the exciton resonance of WS_2 monolayer (~615 nm) so that it can be manipulated via the

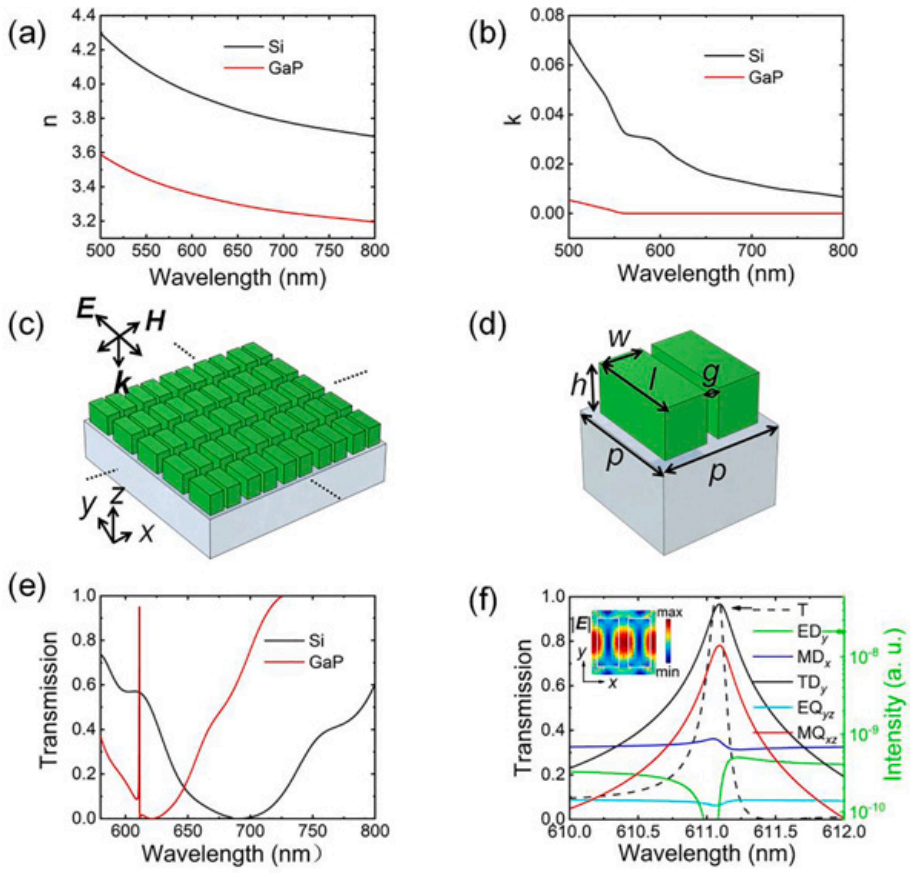

Fig. 1. (a) Comparison of the real parts of the complex refractive indices of GaP and Si in the visible light spectrum. (b) Comparison of the imaginary parts of the complex refractive indices of GaP and Si in the visible light spectrum. (c) Configuration of a GaP metasurface located on a SiO_2 substrate. (d) Unit cell of the GaP metasurface composed of two GaP cuboids. Here, the length, width and height of each GaP cuboid are demote by *l*, *w*, and *h*. The gap width between the two GaP cuboids is denoted by *g* while the period of the regular array of GaP cuboids is denoted by *p*. (e) BIC revealed in the transmission spectrum of a GaP metasurface with $p = 310$ nm, $l = 240$ nm, $w = 110$ nm, $h = 150$ nm, and $g = 40$ nm. The transmission spectrum of a Si metasurface with the same structural parameters is also provided for comparison. (f) Transmission (T) spectrum and multipolar expansion analysis in a logarithmic coordinate of the BIC supported by the GaP metasurface. The electric field distribution in the GaP "molecule" is shown in the inset.

injection of excitons and trions into the WS_2 monolayer, as demonstrated later. The Q factor of the optical resonance is found to be ~ 3635. If we replace the GaP cuboids with Si cuboids, the high-Q optical resonance disappears completely owing to the larger extinction coefficient of Si (see Fig. 1e). It indicates that the imaginary part of the complex refractive index of the dielectric material plays a crucial role in the formation of high-Q optical resonances. From this viewpoint, GaP is a promising candidate for constructing dielectric metasurfaces supporting high-Q BICs in the visible to near infrared spectral range.

We examine the electric field distribution on the top surface of the GaP cuboid, which is important for the coupling with WS_2 monolayer. The electric field distribution in the XY plane is shown in the inset of Fig. 1f. It is found that the electric field is strongly localized in the gap region between the two GaP cuboids with an enhancement factor of ~ 23. The electric field in the gap region is oriented along the Y direction. These features are suitable for the coupling with the excitons in WS_2 monolayer, which oriented in the XY plane. On the other hand, a small variation in the refractive index of WS_2 monolayer will have great impact on the high-Q optical resonance supported by the GaP metasurface. Thus, it offers us the opportunity for optically controlling the transmission properties of the WS_2/GaP metasurface, implying potential applications in all-optical switching.

In order to find out the physical origin of the high-Q optical resonance, we performed a multipolar expansion analysis for it, as shown in Fig. 1f. The formulas used to derive the Mie resonances involved in the interference are expressed as follows [28]:

$$ED = \frac{1}{i\omega}\int j d^3r \tag{2a}$$

$$MD = \frac{1}{2c}\int (r \times j) d^3r \tag{2b}$$

$$TD = \frac{1}{10c}\int [(r \bullet j)r - 2(r \bullet r)j] d^3r, \tag{2c}$$

$$\mathrm{EQ}_{\alpha\beta} = \frac{1}{i2\omega}\int \left[r_\alpha j_\beta + r_\beta j_\alpha - \frac{2}{3}(r \cdot j)\delta_{\alpha\beta} \right] d^3r, \tag{2d}$$

$$\mathrm{MQ}_{\alpha\beta} = \frac{1}{3c}\int \left[(r \times j)_\alpha r_\beta + (r \times j)_\beta r_\alpha \right] d^3r \tag{2e}$$

Here, *c* is the speed of light in vacuum, α and β represent the Cartesian coordinate components *x*,*y*, and *z*. In Eq. (2), the current density is given by:

$$J(r) = -i\omega\varepsilon_0 \left[\varepsilon_r(r) - \varepsilon_{r,d} \right] E(r). \tag{3}$$

The radiated power of the multipolar moments was calculated as follows:

$$I_p = \frac{\mu_0\omega^4}{12\pi c}|\vec{p}|^2,\ I_m = \frac{\mu_0\omega^4}{12\pi c}|\vec{m}|^2,\ I_T = \frac{\mu_0\omega^4 k^2}{12\pi c}|\vec{T}|^2,\ I_{EQ} = \frac{\mu_0\omega^4 k^2}{40\pi c}\sum |EQ_{\alpha\beta}|^2,\ I_{MQ} = \frac{\mu_0\omega^4 k^2}{160\pi c}\sum |MQ_{\alpha\beta}|^2 \tag{4}$$

As shown in Fig. 1f, the high-Q optical resonance originates from the interference of the TD_y and MQ_{xz} modes supported by the GaP "molecule". This behavior is quite similar to that observed in the excitation of a Si nanoparticle dimer by using a radially polarized beam [30]. The only difference is that the Q factor of the optical resonance is significantly enhanced due to the collective interaction of periodically arranged GaP "molecules". It is also revealed that TD_y and MQ_{xz} are the subradiant modes (narrow modes) while MD_x is the superradiant mode (broad mode) in the formation of the Fano resonance. Accordingly, it is found that TD_y and MQ_{xz} can be excited by a MD source oriented along the *x*-axis direction (i.e., MD_x) and placed at the center of the "molecule"

(see Fig. S1).

Previously, the transmission properties of dielectric metasurfaces constructed with dielectric molecules of different materials have been investigated [26,27,37,45–52]. Most studies focus on Si-based metasurfaces supporting high-Q optical resonances in the near infrared spectral range. In these cases, the symmetry of the unit cell is intentionally broken in order to reveal the BIC in the transmission spectrum. For example, the length or width of a constituent cuboid is intentionally reduced [26,27,37,46–51]. In order words, the dielectric "molecule" is composed of two "atoms" with different sizes. It is generally observed that the Q factor of the quasi-BIC decreases rapidly with increasing asymmetry. Here, we show that the symmetry of the GaP "molecule" is not the most important factor that influences the Q factor of the quasi-BIC. Instead, the gap width between the two GaP cuboids plays a crucial role in determining the Q factor of the quasi-BIC.

Now we consider a GaP metasurface with structural parameters p = 310 nm, l = 240 nm, w = 110 nm, and h = 150 nm. In Fig. 2a, we show the transmission spectra calculated for the metasurfaces with different gap widths (g). An optical resonance, which is attributed to the quasi-BIC supported by the metasurface, is observed at ~ 610 nm. It possesses an asymmetric Fano lineshape, implying the existence of mode interference. The quasi-BIC becomes narrower when g approaches 45 nm. It disappears in the transmission spectrum at g = 45 nm because of the large Q factor. In this case, the linewidth of the quasi-BIC (~2.6×10^{-5} nm) is smaller than the wavelength interval (~0.01 nm) used in the calculation of the transmission spectrum. By using a smaller wavelength interval (~1×10^{-5} nm), it can be revealed again in the transmission spectrum of the metasurface, as shown in the inset. In this case, it is noticed that the quasi-BIC possesses an asymmetric Fano lineshape and the transmittance is reduced to ~ 0.50. Now we examine the dependence of the resonant wavelength and the Q factor of the quasi-BIC on the gap width (g) between the two GaP cuboids, as shown in Fig. 2b. It was found that the resonant wavelength of the quasi-BIC remains almost unchanged when g is varied. In sharp contrast, the Q factor of the quasi-BIC is extremely sensitive to the change of g and it exhibits a maximum value of ~ 2.5×10^{7} at g = 45 nm. When g deviates from g = 45 nm, an exponential decrease of the Q factor is observed. For example, the Q factor at g = 45 nm is larger than that at g = 30 or 60 nm by five orders of magnitude. The exponential decrease of the Q factor of the quasi-BIC is quite similar to that observed in previous studies when the asymmetry in the constituent is increased. At first glance, the GaP "molecule" used to construct the GaP metasurface is a symmetric structure. A careful inspection reveals, however, that the gap width on both sides of the GaP cuboid is asymmetric in most cases. For example, the gap widths of the left GaP cuboid with its neighbors are 60 and 30 nm when g is chosen to be 30 nm. When g is set to be 45 nm, the gap widths for each GaP cuboid in the metasurface is equal (45 nm) and the Q factor of the quasi-BIC reaches a maximum. In this case, it is remarkable that the unit cell of the metasurface can be reduced to a single GaP cuboid. However, the quasi-BIC is not observed if we use a single GaP cuboid only as the unit cell to calculate the transmission spectrum of the metasurface. As discussed above, the quasi-BIC originates from the interference of the TD and MQ, which are supported only in a GaP "molecule" rather than a single GaP "atom". From the electric field distribution shown in the inset of Fig. 2a, it is found that the electric fields in the two GaP cuboids are out of phase. This out-of-phase electric field distribution cannot be achieved in the unit cell composed of a single GaP cuboid. Although this type of BIC is not relevant to the breaking in the geometrical symmetry, we think it still belongs to symmetry-protected BIC because it is closely related to the symmetry of the lattice. In previous studies, it is noticed that the change in the Q factor induced by the increase in asymmetry is usually accompanied with a large shift of the resonant wavelength of the quasi-BIC [27]. In our case, the resonant wavelength of the quasi-BIC remains nearly unchanged when the Q factor is exponentially manipulated by varying the gap width. This is an advantage when the quasi-BIC is employed in the construction of photonic devices.

As shown in Fig. 1f, we performed a multipolar expansion analysis for the transmission spectrum of the metasurface in a logarithmic coordinate and identified the physical origin of the quasi-BIC as the interference of the TD_y and MQ_{xz} supported by the GaP "molecule". In Fig. 2c, we plot the intensities of the constituent Mie resonances as a function of the gap width. It is found that MD_x, which radiates in the z direction, is another Mie resonance that contributes to the quasi-BIC. It is not sensitive to the variation of g. As expected, an exponential increase

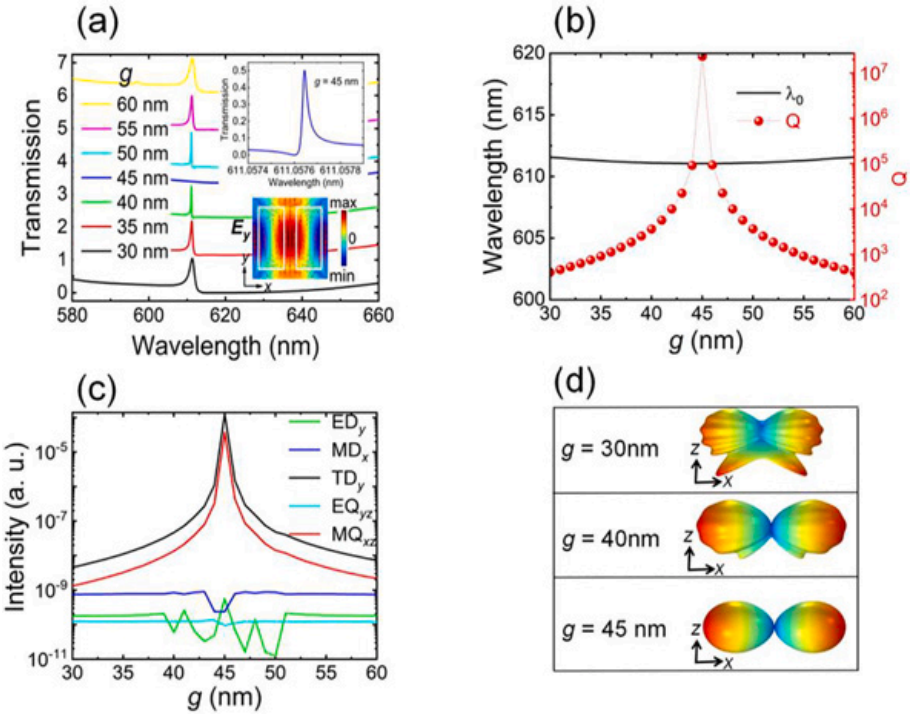

Fig. 2. (a) Transmission spectrum calculated for the metasurfaces with structural parameters of p = 310 nm, l = 240 nm, w = 110 nm, h = 150 nm and different gap widths from 30 to 60 nm. The transmission spectrum with a smaller wavelength interval for the metasurface with g = 45 nm and the corresponding electric field distribution $\boldsymbol{E_y}$ in the XY plane are shown in the insets. (b) Dependences of the resonant wavelength and Q factor of the quasi-BIC on the gap width (g) between the two GaP cuboids. (c) Intensities of the constituent Mie resonances as a function of the gap width. (d) Three-dimensional radiation patterns of the GaP "molecules" with g = 30, 40, 45 nm.

is observed for the TD_y and MQ_{xz} when g approaches 45 nm. A detailed inspection reveals that the ratio of TD_y to MQ_{xz} remains nearly unchanged when g is varied (see Fig. S2). For $g = 45$ nm, MD_x is negligible as compared with TD_y and MQ_{xz} and the destructive interference between them in the z direction leads to a large Q factor of the quasi-BIC. It should be emphasized, however, that MD_x also participates the formation of the quasi-BIC in this case. Being as a superradiant mode with a broad linewidth, the interaction of MD_x with TD_y/MQ_{xz} (subradiant modes) leads to an asymmetric Fano lineshape and a reduction of the transmission (see the inset of Fig. 2a). For $g = 30$ or 60 nm, it is noticed that the intensity difference between MD_x and TD_y/MQ_{xz} is less than one order of magnitude. Since MD_x is a radiant mode, the quasi-BIC becomes more loss and possesses a much smaller Q factor of only $\sim 10^2$. The electric field enhancement, which is important for practical applications, is dramatically reduced when the Q factor of the quasi-BIC is decreased. For $g = 45$ nm, an enhancement factor as large as $|\boldsymbol{E}|/|\boldsymbol{E}_0| \sim 1140$ is achieved. However, this value is reduced to ~ 23 when $g = 40$ nm.

In order to gain a deep insight into the radiation of the quasi-BIC, we simulated the three-dimensional radiation patterns of the GaP "molecules" with different gap widths, as shown in Fig. 2d. For $g = 30$ nm, the radiation pattern is dominated by the radiation in the x direction. However, there exists a severe leakage into the substrate. For $g = 40$ nm, the leakage into the substrate is reduced significantly and an 8-shaped radiation pattern is observed. For $g = 45$ nm, the radiation in the z direction (i.e., out-of-plane radiation) disappears completely and a perfect 8-shaped radiation pattern is achieved.

In order to understand the correlation between the radiation pattern and the interference of TD_y and MQ_{xz}, we present the radiation patterns of TD_y and MQ_{xz} in Fig. 3a. The radiation pattern of TD_y appears as a doughnut while that of MQ_{xz} appears as a flower lobe. The interference of TD_y and MQ_{xz} leads to the cancellation of the radiation in the z direction and the enhancement of the radiation in the x direction. Consequently, an 8-shaped radiation pattern is obtained. The coupling between the neighboring unit cells results in a surface wave propagating in the metasurface. If g is chosen appropriately, the radiation loss of the surface wave is quite small, leading to an extremely large Q factor, as schematically shown in Fig. 3b. It was found that the symmetric gap widths on both sides of each GaP cuboid can also be realized by changing the period of the metasurface or the width of the GaP cuboid when the other parameters are fixed (see Fig. S3a-d). Anyway, the largest Q factor is achieved when the gap widths on both sides of each GaP cuboid is equal.

3.2. Dependence of the BIC on the polarization of the excitation light

The quasi-BIC discussed above appears in the transmission spectrum of the metasurface when it is excited by using a plane wave polarized along the y direction. If we excite the metasurface with a normally incident plane wave polarized along the x direction, we can obtain a quasi-BIC located at $\sim$ 580 nm, as shown in Fig. 4a. In this case, the quasi-BIC appears as a Fano dip in the transmission spectrum. Based on the multipolar expansion analysis, it is revealed that the quasi-BIC is formed by the interference of MD_y and EQ_{xz}. Similarly, the subradiant and superradiant modes involved in the formation of the Fano resonance are identified as MD_y/EQ_{xz} and ED_x. In addition, it is verified that MD_y/EQ_{xz} can indeed be excited by an ED source oriented along the x-axis direction (i.e., ED_x) placed at the center of the "molecule" (see Fig. S4). The interference of the MD_y and EQ_{xz} modes leads to the cancellation of the radiation in the z direction, exhibiting a perfect 8-shaped radiation pattern in the x direction. This behavior is quite similar to that observed in the quasi-BIC shown in Fig. 3. In Fig. 4b, we present the evolution of the transmission spectrum of the metasurface with increasing gap width (g value). Similarly, the largest Q factor is observed for the quasi-BIC in the metasurface with $g = 45$ nm. If we examine the z component of the electric field (see the inset), it is found that the electric fields in the two GaP cuboids are out-of phase. This behavior indicates the existence of two anti-parallel EDs in the z direction, forming an EQ mode (EQ_{xz}). In Fig. 4c, we show the dependences of the resonant wavelength and Q factor of the quasi-BIC on the gap width. Still, the resonant wavelength is not sensitive to the change of the gap width. In sharp contrast, an exponential decrease of the Q factor is observed when g deviates from $g = 45$ nm where the largest Q factor is achieved. In Fig. 4d, we plot the intensities of the three Mie resonances (ED_x, MD_y, and EQ_{xz}) involved in the formation of the quasi-BIC based on the multipolar expansion analysis. It is noteworthy that the intensities of the MD_y and EQ_{xz} depend exponentially on the gap width and the ratio between them remains almost unchanged (see Fig. S5). In comparison, the ED_x participating the interference is not sensitive to the variation of the gap width. Thus, it is easily understood why the largest Q factor is achieved at $g = 45$ nm. We examine the radiation patterns for the GaP "molecules" with different g values, as shown in Fig. 4e. For $g = 30$ nm, the radiation pattern is dominated by the 8-shaped one originating from the interference between MD_y and EQ_{xz}. The existence of ED_x leads to the leakage into the

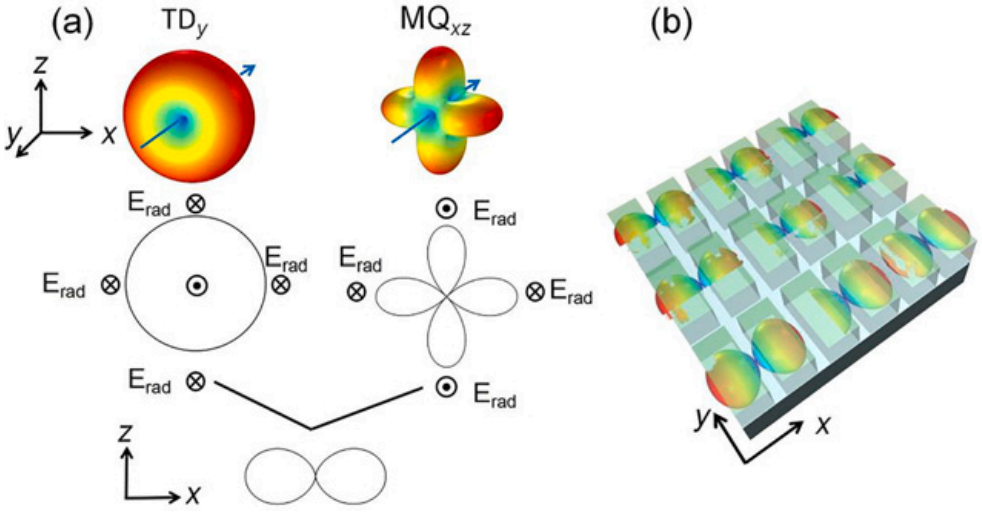

Fig. 3. (a) Three-dimensional (upper panel) and two-dimensional (middle panel) radiation patterns of the TD_y amd MQ_{xz} modes in the xz plane, and the two-dimensional radiation pattern in the xz plane resulting from the interference of them (lower panel). (b) Surface wave resulting from the coupling of the radiations of GaP molecules and propagating in the xy plane.

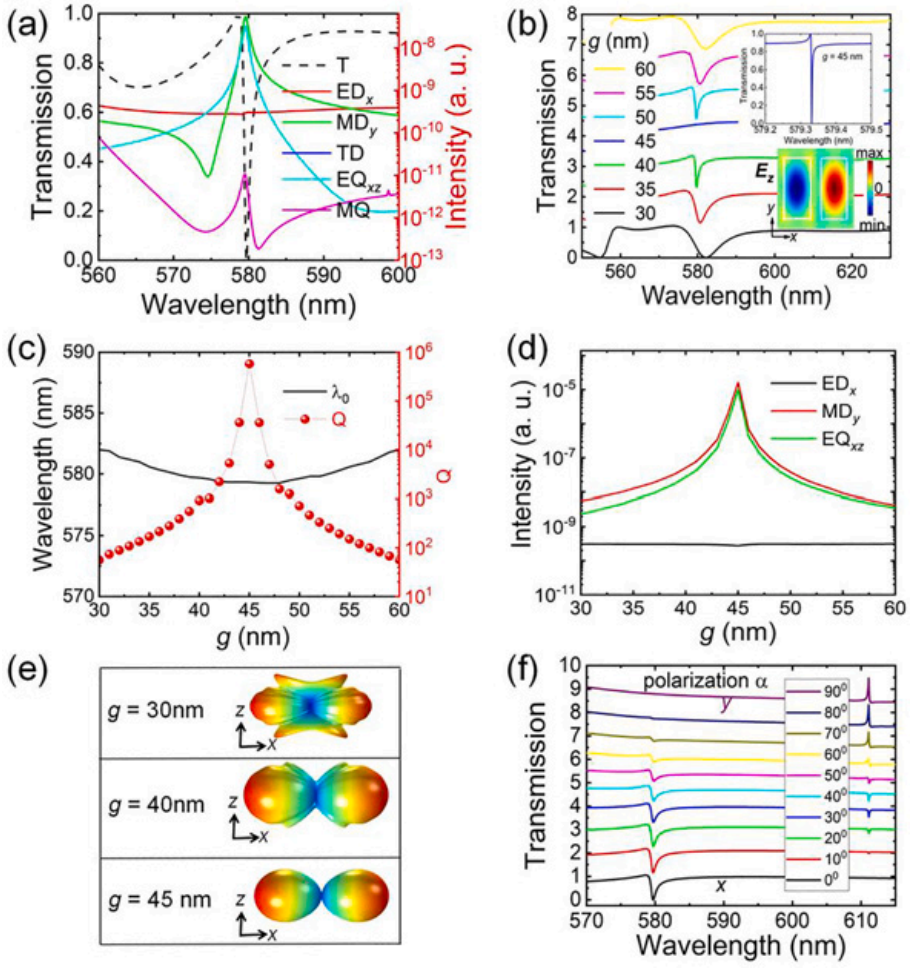

Fig. 4. (a) Transmission (T) spectrum calculated for a metasurface with p = 310 nm, l = 240 nm, w = 110 nm, h = 150 nm, g = 40 nm. The Mie resonances contributing in a logarithmic coordinate to the transmission are also provided. (b) Transmission spectra calculated for metasurfaces with different g values. The transmission spectrum with a smaller wavelength interval for the metasurface with g = 45 nm and the corresponding electric field distribution $\boldsymbol{E}_z$ in the XY plane are shown in the insets. (c) Dependences of the resonant wavelength and the Q factor of the quasi-BIC on the gap width (g value). (d) Intensities of the Mie resonances involved in the interference as a function of the gap width (g value). (e) Radiation patterns calculated for the metasurfaces with different gap widths (g values). (f) Transmission spectra of the metasurface excited by using plane waves with different polarization angles ranging from 0° to 90°.

substrate and air. When g is increased to 40 nm, the leakage is greatly reduced. At g = 45 nm, the leakage in the z direction disappears completely and a perfect 8-shaped radiation pattern is observed. In order to understand the correlation between the radiation pattern and the interference of MD$_y$ and EQ$_{xz}$, we present the radiation patterns of MD$_y$ and EQ$_{xz}$ (see Fig. S6). In Fig. 4f, we show the transmission spectra calculated for the metasurface excited by using plane waves with different polarization angles ranging from 0° to 90°. Here, the polarization angle is defined as the angle between the polarization direction and the x axis. Except for 0° and 90°, one can see two quasi-BICs in the transmission spectrum of the metasurface. Apparently, the resonant wavelengths of the two quasi-BICs are determined by the length and width of the GaP cuboids. Therefore, one can adjust the wavelengths of the two quasi-BICs for practical applications. For example, the wavelengths of the two-BICs can be designed at the resonant wavelengths of the two excitons (A and B excitons) of WS_2 monolayer by appropriately choosing the length and width of the GaP cuboid.

3.3. Optical sensing based on the quasi-BIC

Apparently, the high-Q BICs supported by GaP metasurfaces can be employed to realize optical sensing with high sensitivities. In general, the sensitivity (S) of a sensor with a unit of nm/RIU is defined as [34,35]:

$$S = \Delta\lambda_{BIC}/\Delta n \tag{5a}$$

Here, $\Delta\lambda_{\mathrm{BIC}}$ is the wavelength shift of the BIC induced by the variation of refractive index of Δn. The corresponding FOM is calculated by

$$\mathrm{FOM} = \frac{S}{W} = \frac{SQ}{\lambda_{BIC}} \tag{5b}$$

Here, λ_{BIC}, W *and* Q denote the resonant wavelength, linewidth and Q factor of the BIC.

As an example, we first calculated the sensitivity of the metasurface shown in Fig. 1. In Fig. 5a, we show the evolution of the quasi-BIC in the metasurface excited by using x-polarized plane wave when the refractive index of the environment is changed from n = 1.00 to n = 1.10. It can be seen that the wavelength of the quasi-BIC is shifted from ~ 580 nm to ~ 593.5 nm. If we plot the wavelength of the quasi-BIC as a function of the refractive index, a linear relationship is observed, as shown in Fig. 5c. The sensitivity extracted from the linear fitting of the relationship is S = 135 nm/RIU. Similarly, we examine the evolution of the quasi-BIC in the metasurface excited by using y-polarized plane wave, as shown in Fig. 5b. The quasi-BIC is shifted from ~ 611 to ~ 620 nm when the refractive index of the environment is changed from n = 1.00 to n = 1.20. As expected, a linear relationship between the wavelength of the quasi-BIC and the refractive index is also observed, as shown in Fig. 5d. In this case, the sensitivity is found to be S = 45 nm/RIU.

In Eq. (5b), it can be seen that the FOM of the sensor is proportional to the Q factor of the quasi-BIC, implying that the FOM can be improved by using a quasi-BIC with a large Q factor. We also examined the dependence of the resonant wavelength of the quasi-BIC on the refractive index of the surrounding environment for metasurfaces with different gap widths (see Fig. S7). It was found that the sensors made of different metasurfaces exhibit almost the same sensitivity. In Fig. 5e and

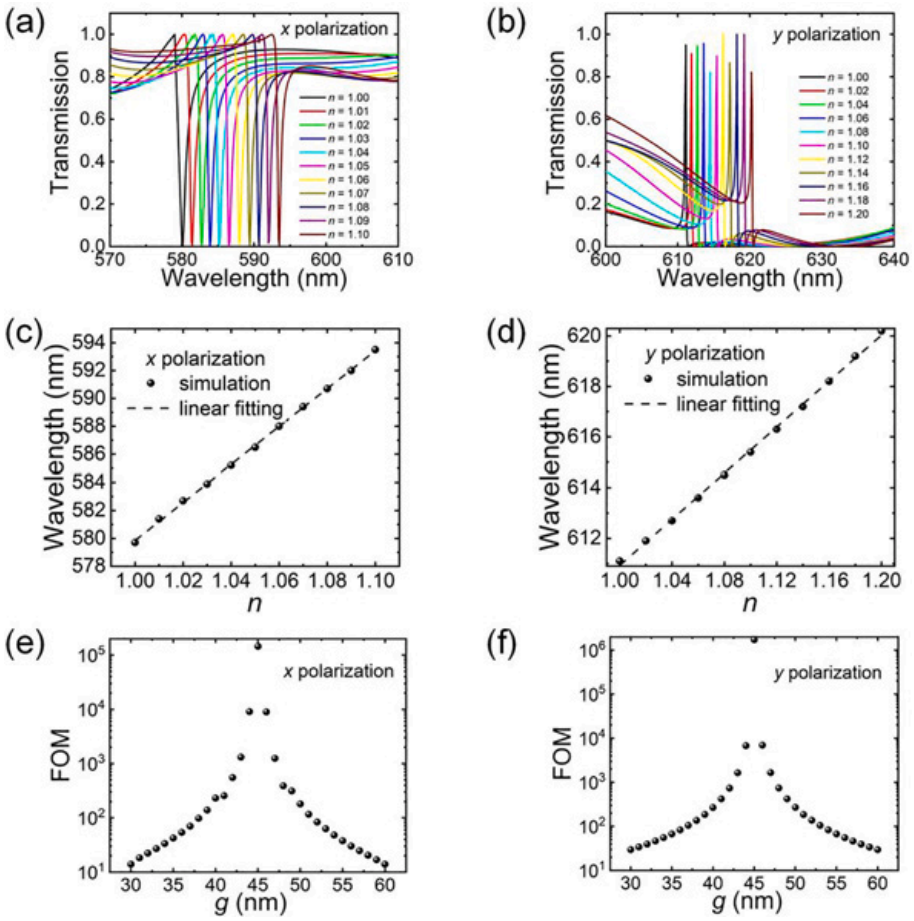

Fig. 5. Transmission spectra calculated for a metasurface (p = 310 nm, l = 240 nm, w = 110 nm, h = 150 nm, g = 40 nm) in background media with different refractive indices n. The results obtained by using plane waves polarized along the $\times$ and y directions are shown in (a) and (b), respectively. The corresponding dependences of the resonant wavelength of the quasi-BIC on the background refractive index are shown in (c) and (d) for x-polarization and y-polarization, respectively. The dependences of the FOM on the gag width (g) are shown in (e) and (f) for x- and y-polarized white light, respectively.

5f, we show the FOMs obtained for metasurfaces with different gap widths excited by using x- and y-polarized white light, respectively. It can be seen that the FOMs of the sensor increases exponentially when the gap width approaches g = 45 nm. The maximum FOM exceeds 10^5 and 10^6 when x- and y-polarized white light is employed.

3.4. Optical switching based on the quasi-BIC

The manipulation of the Q factor of the quasi-BIC by changing the structural parameters (such as the gap width, the period, and the cuboid width etc.) is static and it can only be realized in the fabrication process. For device applications, it is highly desirable to realize dynamical control and manipulation of the Q factor of the quasi-BIC. As discuss at the beginning, the active control of the optical properties of a dielectric metasurface can be realized by attaching a two-dimensional material on the metasurface, forming a hybrid metasurface. The main purpose of this work is to design a dielectric metasurface operating in the visible light spectrum, which can be integrated with two-dimensional materials. It is found that GaP is one of the most promising candidates for achieving this goal because it possesses a refractive index comparable to Si and negligible extinction coefficient for wavelengths longer than 550 nm. In this work, we proposed the use of a WS_2 monolayer loaded on a GaP metasurface to construct a WS_2/GaP hybrid metasurface owing to its unique optical properties, as schematically shown in Fig. 6a. A WS_2 monolayer, which is generally fabricated by chemical vapor deposition technique, is transferred from a Si substrate to the top surface of the GaP metasurface, forming a WS_2/GaP hybrid metasurface. It has been known that the A exciton of WS_2 monolayer located at ~ 615 nm, which can be revealed in the photoluminescence (PL) spectrum of a WS_2 monolayer as a symmetric Lorentz lineshape. With increasing excitation irradiance, the PL spectrum of the WS_2 monolayer will become asymmetric due to the generation of trions and it will be gradually dominated by the emission of trions [53]. It implies that the imaginary part of the complex refractive index of WS_2 monolayer can be significantly modified by laser irradiation. So does the real part of the complex refractive index based on the Kromer-Kronig relation. This unique feature offers us the opportunity for actively manipulating the optical properties (e.g., the quasi-BIC) of the WS_2/GaP hybrid metasurface.

It is well known that the introduction of optical loss will lead to the collapses of high-Q optical resonances. Thus, the wavelength of the quasi-BIC of the GaP metasurface cannot be designed at the exciton resonance of the WS_2 monolayer. On the other hand, we hope to control the quasi-BIC by using the trions generated by laser irradiation. Therefore, the wavelength of the quasi-BIC is intentionally chosen at the long-wavelength side of the exciton resonance where the trion resonance will be induced by laser light. In order to extract the laser-induced change in the complex permittivity of WS_2 monolayer, we excited a WS_2 monolayer with 488-nm laser light and recorded the PL spectra of the WS_2 monolayer at different laser powers. In each case, the PL can be decomposed into the contributions from excitons and trions by fitting the PL spectrum with two Lorentz lineshapes. In this way, one can derive the resonant wavelengths and damping rates (i.e., linewidths) of the excitons and trions at different laser powers. The oscillator strengths of the excitons and trions can be extracted by fitting the scattering spectra of a Si/WS_2/Au nanocavities excited by laser light with different powers [53]. By using the above parameters used to characterize the excitons and trions, one can derive the complex permittivity at different laser powers by using the following expression:

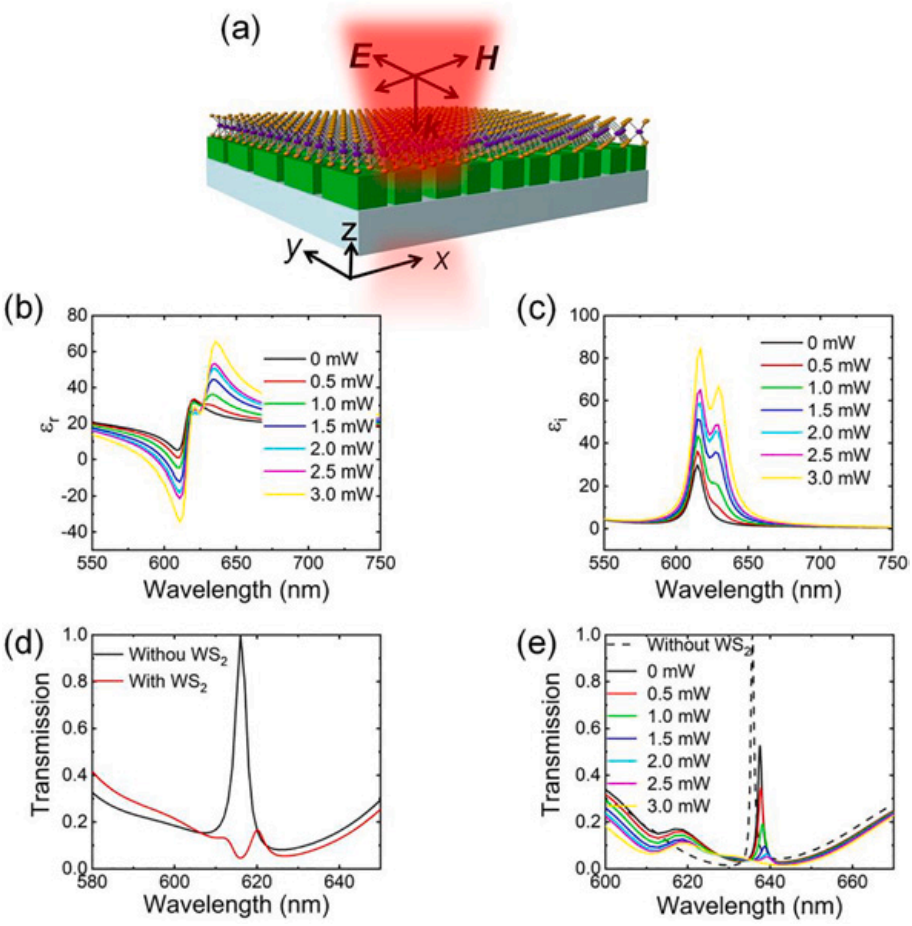

Fig. 6. (a) Schematic showing the configuration of a WS_2/GaP hybrid metasurface excited by a laser beam. (b) Real parts of the complex dielectric constants extracted for WS_2 monolayer at different laser powers. (c) Imaginary parts of the complex dielectric constants extracted for WS_2 monolayer at different laser powers. (d) Transmission spectra calculated for the Metasurface without and with an attached WS_2 monolayer (p = 310 nm, l = 240 nm, w = 113 nm, h = 140 nm, g = 20 nm). (e) Transmission spectra calculated for the WS_2/GaP hybrid metasurface irradiated by using a 488-nm laser beam with different powers (p = 310 nm, l = 240 nm, w = 118 nm, h = 150 nm, g = 50 nm).

$$\varepsilon = \varepsilon_\infty + \sum_i \frac{f_i \omega_i^2}{\omega_i^2 - \omega^2 - i\gamma_i \omega} \tag{6}$$

where ε_∞ is the dielectric function of background, f_i, ω_i and γ_i ($i = A^-, A, B, C$) are the oscillator strengths, central frequencies, and damping rates of the excitons and trions, respectively.

In Fig. 6b,c, we show the real and imaginary parts of the complex permittivity derived for WS_2 monolayer at different laser powers [53]. It is noticed that both of them can be greatly modified by laser irradiation. In Fig. 6d, we show the transmission spectrum of a WS_2/GaP metasurface with p = 310 nm, l = 240 nm, w = 113 nm, h = 140 nm, g = 20 nm. The transmission spectrum of the GaP metasurface in the absence of the WS_2 monolayer is also provided for reference. In this case, the quasi-BIC with a Q factor of 206 is designed to be resonant with the exciton resonance of WS_2 monolayer. The interaction between them results in the formation of two hybrid states, which are manifested as two transmission peaks with much smaller intensities. The Rabi splitting is found to be ~ 26 meV while the averaged damping rate of the quasi-BIC and the exciton resonance is estimated to be ~ 8 meV and ~ 45 meV, respectively. Apparently, the strong coupling criterion is not satisfied in this case because of the large difference in the damping rate (or linewidth) between the two modes. If we intentionally design the quasi-BIC at the long-wavelength side of the exciton resonance by using a GaP metasurface with p = 310 nm, l = 240 nm, w = 118 nm, h = 150 nm, g = 50 nm, then the quasi-BIC of the WS_2/GaP hybrid metasurface will survive with a reduced intensity, as shown in Fig. 6e. Based on the laser-power-dependent complex permittivity presented in Fig. 6b,c, we calculated the transmission spectra of the WS_2/GaP hybrid metasurface under the irradiation of laser light with different powers, as shown in Fig. 6e. It can be seen that the quasi-BIC is attenuated with increasing laser power, implying the possibility for realizing the active control of the quasi-BIC.

4. Conclusions

In summary, we proposed the use of a GaP "molecule" composed of two identical GaP cuboids as the unit cell to construct a metasurface that supports a quasi-BIC in the visible light spectrum. It was revealed that the quasi-BIC is formed by the interference of the TD_y and MQ_{xz} modes supported by the GaP "molecule" when the metasurface is excited by a y-polarized plane wave or by the interference of the MD_y and EQ_{xz} modes when the metasurface is excited by a x-polarized plane wave. It was found that the gap width is an important structural parameter that determines the Q factor of the quasi-BIC and the largest Q factor is achieved in the metasurface in which the gap widths on both sides of each GaP cuboid are equal. We unveiled the underlying physical mechanism based on the mode interference theory. We showed that the high-Q quasi-BIC supported by the metasurface can be used as high performance sensors. We demonstrated the active control of the quasi-BIC in the WS_2/GaP metasurface by utilizing the refractive index change in the WS_2 monolayer induced by injecting excitons and trions into the WS_2 monolayer with laser light. Our findings open an avenue for designing dielectric metasurfaces operating in the visible spectrum and pave the way for constructing novel photonic devices based on hybrid metasurfaces.

CRediT authorship contribution statement

Zhaotang Li: Conceptualization, Data curation, Formal analysis, Investigation, Methodology, Writing – original draft, Writing – review &

editing. **Mingcheng Panmai:** Formal analysis, Data curation. **Lidan Zhou:** Formal analysis. **Shulei Li:** Formal analysis. **Shimei Liu:** Visualization. **Jianhua Zeng:** Visualization. **Sheng Lan:** Conceptualization, Formal analysis, Funding acquisition, Investigation, Methodology, Project administration, Resources, Supervision, Validation, Writing – original draft, Writing – review & editing.

Declaration of Competing Interest

The authors declare that they have no known competing financial interests or personal relationships that could have appeared to influence the work reported in this paper.

Data availability

Data will be made available on request.

Acknowledgement

This work was financially supported by the National Natural Science Foundation of China (Grant Nos. 11874020 and 12174123).

Appendix A. Supplementary material

Supplementary data to this article can be found online at https://doi.org/10.1016/j.apsusc.2023.156779.

References

[1] M. Decker, I. Staude, M. Falkner, J. Dominguez, D.N. Neshev, I. Brener, T. Pertsch, Y.S. Kivshar, High-Efficiency Dielectric Huygens' Surfaces, Adv. Optical Mater. 3 (2015) 813–820.
[2] Y. Yang, D.P. Kravchenko II, J.V. Briggs, All-dielectric metasurface analogue of electromagnetically induced transparency, Nat. Commun. 5 (2014) 5753.
[3] L. Wang, S. Kruk, K. Koshelev, I. Kravchenko, B. Luther-Davies, Y. Kivshar, Nonlinear Wavefront Control with All-Dielectric Metasurfaces, Nano Lett. 18 (2018) 3978–3984.
[4] K.E. Chong, I. Staude, A. James, J. Dominguez, S. Liu, S. Campione, G. S. Subramania, T.S. Luk, M. Decker, D.N. Neshev, I. Brener, Y.S. Kivshar, Polarization-Independent Silicon Metadevices for Efficient Optical Wavefront Control, Nano Lett. 15 (2015) 5369–5374.
[5] W. Liu, Generalized Magnetic Mirrors, Phys. Rev. Lett. 119 (2017), 123902.
[6] V.A. Fedotov, M. Rose, S.L. Prosvirnin, N. Papasimakis, N.I. Zheludev, Sharp trapped-mode resonances in planar metamaterials with a broken structural symmetry, Phys. Rev. Lett. 99 (2007), 147401.
[7] C. Kyaw, R. Yahiaoui, J.A. Burrow, V. Tran, K. Keelen, W. Sims, E.C. Red, W. S. Rockward, M.A. Thomas, A. Sarangan, I. Agha, T.A. Searles, Polarization-selective modulation of supercavity resonances originating from bound states in the continuum, Commun. Phys. 3 (2020) 00453.
[8] X. Chen, W. Fan, H. Yan, Toroidal dipole bound states in the continuum metasurfaces for terahertz nanofilm sensing, Opt. Express 28 (2020) 17102–17112.
[9] V.R. Tuz, V.V. Khardikov, A.S. Kupriianov, K.L. Domina, S. Xu, H. Wang, H.B. Sun, High-quality trapped modes in all-dielectric metamaterials, Opt. Express 26 (2018) 2905–2916.
[10] A. Forouzmand, H. Mosallaei, All-Dielectric C-Shaped Nanoantennas for Light Manipulation: Tailoring Both Magnetic and Electric Resonances to the Desire, Adv. Optical Mater. 5 (2017) 1700147.
[11] S. Campione, S. Liu, L.I. Basilio, L.K. Warne, W.L. Langston, T.S. Luk, J.R. Wendt, J. L. Reno, G.A. Keeler, I. Brener, M.B. Sinclair, Broken Symmetry Dielectric Resonators for High Quality Factor Fano Metasurfaces, ACS Photonics 3 (2016) 2362–2367.
[12] P.P. Vabishchevich, S. Liu, M.B. Sinclair, G.A. Keeler, G.M. Peake, I. Brener, Enhanced Second-Harmonic Generation Using Broken Symmetry III–V Semiconductor Fano Metasurfaces, ACS Photonics 5 (2018) 1685–1690.
[13] X. Wang, J. Duan, W. Chen, C. Zhou, T. Liu, S. Xiao, Controlling light absorption of graphene at critical coupling through magnetic dipole quasi-bound states in the continuum resonance, Phys. Rev. B 102 (2020), 155432.
[14] Z. Liu, Y. Xu, Y. Lin, J. Xiang, T. Feng, Q. Cao, J. Li, S. Lan, J. Liu, High-Q Quasibound States in the Continuum for Nonlinear Metasurfaces, Phys. Rev. Lett. 123 (2019), 253901.
[15] C. Zhou, X. Qu, S. Xiao, M. Fan, Imaging Through a Fano-Resonant Dielectric Metasurface Governed by Quasi–bound States in the Continuum, Phys. Rev. Applied 14 (2020), 044009.
[16] A.S. Kupriianov, Y. Xu, A. Sayanskiy, V. Dmitriev, Y.S. Kivshar, V.R. Tuz, Metasurface Engineering through Bound States in the Continuum, Phys. Rev. Applied 12 (2019), 014024.
[17] S. Xie, S. Xie, J. Zhan, C. Xie, G. Tian, Z. Li, Q. Liu, Bound States in the Continuum in a T-Shape Nanohole Array Perforated in a Photonic Crystal Slab, Plasmonics 15 (2020) 1261–1271.
[18] S. Xie, S. Xie, G. Tian, Z. Li, J. Zhan, Q. Liu, C. Xie, Bound states in the continuum of nanohole array with symmetry broken in THz, Optik 225 (2021), 165761.
[19] Z. Huang, M. Wang, Y. Li, J. Shang, K. Li, W. Qiu, J. Dong, H. Guan, Z. Chen, H. Lu, Highly efficient second harmonic generation of thin film lithium niobate nanograting near bound states in the continuum, Nanotechnology 32 (2021), 325207.
[20] S. Cao, H. Dong, J. He, E. Forsberg, Y. Jin, S. He, Normal-Incidence-Excited Strong Coupling between Excitons and Symmetry-Protected Quasi-Bound States in the Continuum in Silicon Nitride-WS_2 Heterostructures at Room Temperature, J Phys. Chem. Lett. 11 (2020) 4631–4638.
[21] A.A. Bogdanov, K.L. Koshelev, P.V. Kapitanova, M.V. Rybin, S.A. Gladyshev, Z. F. Sadrieva, K.B. Samusev, Y.S. Kivshar, M.F. Limonov, Bound states in the continuum and Fano resonances in the strong mode coupling regime, Adv. Photonics 1 (2019), 016001.
[22] M.V. Rybin, K.L. Koshelev, Z.F. Sadrieva, K.B. Samusev, A.A. Bogdanov, M. F. Limonov, Y.S. Kivshar, High-Q Supercavity Modes in Subwavelength Dielectric Resonators, Phys. Rev. Lett. 119 (2017), 243901.
[23] L. Carletti, K. Koshelev, C. De Angelis, Y. Kivshar, Giant Nonlinear Response at the Nanoscale Driven by Bound States in the Continuum, Phys. Rev. Lett. 121 (2018), 033903.
[24] L. Huang, L. Xu, M. Rahmani, D. Neshev, A.E. Miroshnichenko, Pushing the limit of high-Q mode of a single dielectric nanocavity, Adv. Photonics 3 (2021), 016004.
[25] A.I. Ovcharenko, C. Blanchard, J.-P. Hugonin, C. Sauvan, Bound states in the continuum in symmetric and asymmetric photonic crystal slabs, Phys. Rev. B 101 (2020), 155303.
[26] K. Koshelev, A. Bogdanov, Y. Kivshar, Meta-optics and bound states in the continuum, Sci. Bull. 64 (2019) 836–842.
[27] K. Koshelev, S. Lepeshov, M. Liu, A. Bogdanov, Y. Kivshar, Asymmetric Metasurfaces with High-Q Resonances Governed by Bound States in the Continuum, Phys. Rev. Lett., 121 (2018) 193903.
[28] Y. He, G. Guo, T. Feng, Y. Xu, A.E. Miroshnichenko, Toroidal dipole bound states in the continuum, Phys. Rev. B 98 (2018), 161112.
[29] M. Panmai, J. Xiang, Z. Sun, Y. Peng, H. Liu, H. Liu, Q. Dai, S. Tie, S. Lan, All-silicon-based nano-antennas for wavelength and polarization demultiplexing, Opt. Express 26 (2018) 12344–12362.
[30] F. Deng, H. Liu, M. Panmai, S. Lan, Sharp bending and power distribution of a focused radially polarized beam by using silicon nanoparticle dimers, Opt. Express 26 (2018) 20051–20062.
[31] J. Xiang, J. Chen, S. Lan, A.E. Miroshnichenko, Nanoscale Optical Display and Sensing Based on the Modification of Fano Lineshape, Adv. Optical Mater. 8 (2020) 2000489.
[32] Y.K. Srivastava, R.T. Ako, M. Gupta, M. Bhaskaran, S. Sriram, R. Singh, Terahertz sensing of 7 nm dielectric film with bound states in the continuum metasurfaces, Appl. Phys. Lett. 115 (2019), 151105.
[33] J. Wang, J. Kühne, T. Karamanos, C. Rockstuhl, S.A. Maier, A. Tittl, All-Dielectric Crescent Metasurface Sensor Driven by Bound States in the Continuum, Adv. Funct. Mater. 31 (2021) 2104652.
[34] D.N. Maksimov, V.S. Gerasimov, S. Romano, S.P. Polyutov, Refractive index sensing with optical bound states in the continuum, Opt. Express 28 (2020) 38907–38916.
[35] S. Romano, G. Zito, S. Torino, G. Calafiore, E. Penzo, G. Coppola, S. Cabrini, I. Rendina, V. Mocella, Label-free sensing of ultralow-weight molecules with all-dielectric metasurfaces supporting bound states in the continuum, Photonics Res. 6 (2018) 070726–070733.
[36] W. Cen, T. Lang, J. Wang, M. Xiao, High-Q Fano Terahertz resonance based on bound states in the continuum in All-dielectric metasurface, Appl. Surf. Sci. 575 (2022), 151723.
[37] N. Bernhardt, K. Koshelev, S.J.U. White, K.W.C. Meng, J.E. Froch, S. Kim, T. T. Tran, D.Y. Choi, Y. Kivshar, A.S. Solntsev, Quasi-BIC Resonant Enhancement of Second-Harmonic Generation in WS_2 Monolayers, Nano Lett. 20 (2020) 5309–5314.
[38] T. Wang, S. Zhang, Large enhancement of second harmonic generation from transition-metal dichalcogenide monolayer on grating near bound states in the continuum, Opt. Express 26 (2018) 322–337.
[39] Y. Chen, S. Miao, T. Wang, D. Zhong, A. Saxena, C. Chow, J. Whitehead, D. Gerace, X. Xu, S.F. Shi, A. Majumdar, Metasurface Integrated Monolayer Exciton Polariton, Nano Lett. 20 (2020) 5292–5300.
[40] S. Han, L. Cong, Y.K. Srivastava, B. Qiang, M.V. Rybin, A. Kumar, R. Jain, W. X. Lim, V.G. Achanta, S.S. Prabhu, Q.J. Wang, Y.S. Kivshar, R. Singh, All-Dielectric Active Terahertz Photonics Driven by Bound States in the Continuum, Adv. Mater. 31 (2019) 1901921.
[41] K. Fan, I.V. Shadrivov, W.J. Padilla, Dynamic bound states in the continuum, Optica 6 (2019) 202169–1200173.
[42] S. Murai, D.R. Abujetas, G.W. Castellanos, J.A. Sánchez-Gil, F. Zhang, J.G. Rivas, Bound States in the Continuum in the Visible Emerging from out-of-Plane Magnetic Dipoles, ACS Photonics 7 (2020) 2204–2210.
[43] D.E. Aspnes, A.A. Studna, Dielectric functions and optical parameters of Si, Ge, GaP, GaAs, GaSb, InP, InAs, and InSb from 1.5 to 6.0 eV, Phys. Rev. B, 27 (1983) 985–1009.
[44] A.P. Anthur, H. Zhang, R. Paniagua-Dominguez, D.A. Kalashnikov, S.T. Ha, T.W. W. Mass, A.I. Kuznetsov, L. Krivitsky, Continuous Wave Second Harmonic Generation Enabled by Quasi-Bound-States in the Continuum on Gallium Phosphide Metasurfaces, Nano Lett. 20 (2020) 8745–8751.

[45] G. Sun, S. Peng, X. Zhang, Y. Zhu, Switchable Electromagnetically Induced Transparency with Toroidal Mode in a Graphene-Loaded All-Dielectric Metasurface, Nanomaterials 10 (2020) 1064.
[46] M. Qin, S. Xiao, W. Liu, M. Ouyang, T. Yu, T. Wang, Q. Liao, Strong coupling between excitons and magnetic dipole quasi-bound states in the continuum in WS_2-TiO_2 hybrid metasurfaces, Opt. Express 29 (2021) 18026–18036.
[47] S. Xiao, X. Wang, J. Duan, T. Liu, T. Yu, Engineering light absorption at critical coupling via bound states in the continuum, Opt. Soc. Am. B 38 (2021) 1325–1330.
[48] Z. Zheng, Y. Zhu, J. Duan, M. Qin, F. Wu, S. Xiao, Enhancing Goos-Hanchen shift based on magnetic dipole quasi-bound states in the continuum in all-dielectric metasurfaces, Opt. Express 29 (2021) 29541–29549.
[49] K. Koshelev, Y. Tang, K. Li, D.-Y. Choi, G. Li, Y. Kivshar, Nonlinear Metasurfaces Governed by Bound States in the Continuum, ACS Photonics 6 (2019) 1639–1644.
[50] A. Ndao, L. Hsu, W. Cai, J. Ha, J. Park, R. Contractor, Y. Lo, B. Kanté, Differentiating and quantifying exosome secretion from a single cell using quasi-bound states in the continuum, NANO 9 (2020) 10811–110086.
[51] G. Zograf, K. Koshelev, A. Zalogina, V. Korolev, R. Hollinger, D.-Y. Choi, M. Zuerch, C. Spielmann, B. Luther-Davies, D. Kartashov, S.V. Makarov, S.S. Kruk, Y. Kivshar, High-Harmonic Generation from Resonant Dielectric Metasurfaces Empowered by Bound States in the Continuum, ACS Photonics 9 (2022) 567–574.
[52] E. Mikheeva, K. Koshelev, D.Y. Choi, S. Kruk, J. Lumeau, R. Abdeddaim, I. Voznyuk, S. Enoch, Y. Kivshar, Photosensitive chalcogenide metasurfaces supporting bound states in the continuum, Opt. Express 27 (2019) 338473–1333853.
[53] S. Liu, F. Deng, W. Zhuang, X. He, H. Huang, J.D. Chen, H. Pang, S. Lan, Optical Introduction and Manipulation of Plasmon-Exciton-Trion Coupling in a Si/WS_2/Au Nanocavity, ACS Nano 16 (2022) 14390–14401.